


RESEARCH ARTICLE

Study and optimization of alternative MBE-deposited metallic precursors for highly efficient kesterite CZTSe:Ge solar cells

Sergio Giraldo¹  | Shinho Kim² | Jacob Antonio Andrade-Arvizu¹ | Xavier Alcobé³ |
 Claudia Malerba⁴ | Matteo Valentini⁴ | Hitoshi Tampo² | Hajime Shibata² |
 Victor Izquierdo-Roca¹ | Alejandro Pérez-Rodríguez^{1,5} | Edgardo Saucedo¹

¹ Catalonia Institute for Energy Research (IREC), Jardins de les Dones de Negre 1, Sant Adrià de Besòs (Barcelona) 08930, Spain

² AIST, National Institute of Advanced Industrial Science and Technology, Tsukuba, Japan

³ Centres Científics i Tecnològics de la Universitat de Barcelona (CCiTUB), Lluís Solé i Sabarís 1-3, Barcelona 08028, Spain

⁴ ENEA Casaccia Research Center, via Anguillarese 301, Rome 00123, Italy

⁵ IN2UB, Departament d'Electrònica, Universitat de Barcelona, Martí i Franquès 1, Barcelona 08028, Spain

Correspondence

Sergio Giraldo, Catalonia Institute for Energy Research (IREC), Jardins de les Dones de Negre 1, Sant Adrià de Besòs 08930, Barcelona, Spain.

Email: sgiraldo@irec.cat

Funding information

Agència de Gestió d'Ajuts Universitaris i de Recerca, Generalitat de Catalunya, Grant/Award Number: Ref. 2017 SGR 862; H2020 Societal Challenges, Grant/Award Number: 720907; Secretaría de Estado de Investigación, Desarrollo e Innovación, Grant/Award Numbers: ENE2016-80788-C5-1-R and ENE2017-87671-C3-1-R; FPI fellowship, Grant/Award Number: BES-2014-068533; European Regional Development Funds, Grant/Award Number: Programa Competitivitat de Catalunya 2007-2013; H2020 Programme, Grant/Award Number: H2020-NMBP-03-2016-720907

Abstract

Nowadays, most of the best efficiencies of $\text{Cu}_2\text{ZnSn}(\text{S,Se})_4$ (CZTSSe) solar cells are obtained from absorber layers fabricated using sequential processes, including the deposition of metallic stack precursors, typically by sputtering, and followed by reactive annealing under chalcogen atmosphere. The sputtering technique is widely known for the easy growth of metallic layers, although the deposition rates, growth morphology and nucleation, or the roughness can sometimes be an issue leading to inhomogeneities in the final layers. Nevertheless, MBE (molecular beam epitaxy) technique could have some advantages to obtain high-quality metallic layers, with accurate control of the growth due to ultra-high vacuum conditions and high purity. In this work, we study the use of advanced MBE systems to grow metallic stack precursors, alternatively to sputtering or thermal evaporation techniques, to obtain high-quality CZTSe:Ge absorbers. Due to differences in the nature of each type of precursor, thermal annealing optimizations are presented by modifying some critical selenization parameters, such as the temperature or the selenium amount in order to obtain well-crystallized absorbers. Detailed morphological, compositional, and structural characterizations show relevant features of each precursor, mainly related to the formation of MoSe_2 at the back interface, and Se and Sn composition after selenization in different conditions. Regarding the solar cell devices, main efficiency limitations come from V_{OC} and FF, which could be tentatively related to a noncontrolled selenization; different precursor reactivity, porosity, or composition; and different alkali diffusion during the reactive annealing. Finally, in the first optimization, a 9.2% efficiency device has been achieved with promising perspectives for future improvements.

KEYWORDS

$\text{Cu}_2\text{ZnSnSe}_4$, kesterite, MBE, sputtering, thin-film photovoltaics

This is an open access article under the terms of the Creative Commons Attribution License, which permits use, distribution and reproduction in any medium, provided the original work is properly cited.

© 2019 The Authors. *Progress in Photovoltaics: Research and Applications* Published by John Wiley & Sons Ltd.

1 | INTRODUCTION

$\text{Cu}_2\text{ZnSn}(\text{S,Se})_4$ (CZTSSe) semiconductor materials have attracted considerable attention in the last years, being one of the most promising thin film photovoltaic absorbers, primarily through the use of earth abundant elements and low toxicity.^{1–3} This makes kesterites CZTSSe an interesting mid- to long-term alternative to the widely known $\text{CuIn}_{1-x}\text{Ga}_x\text{Se}_2$ (CIGSe), thus allowing reducing the use of scarce elements like In and Ga.⁴ Apart from that, kesterite has several advantageous properties to be a very suitable material for photovoltaic applications: kesterite has p-type conductivity naturally due to intrinsic point defects; it is direct band gap semiconductor with a high absorption coefficient ($\sim 10^4 \text{ cm}^{-1}$);⁵ its band gap can be easily tuned with the ratio S/Se, from 1.0 eV, for the pure selenium $\text{Cu}_2\text{ZnSnSe}_4$ (CZTSe) compound, to 1.5 eV, for the pure sulfur $\text{Cu}_2\text{ZnSnS}_4$ (CZTS)^{6,7}; and it is highly compatible with CIGS technology, sharing several processing steps and techniques. Furthermore, the fact that kesterite absorbers can be synthesized with a large variety of techniques is another advantage to consider, especially for future industrial perspectives.^{8–18}

Regarding the deposition techniques, these are usually classified as vacuum (mostly physical vapor deposition [PVD]-based) and nonvacuum techniques. Vacuum-based methods include coevaporation,⁸ thermal evaporation,⁹ e-beam evaporation,¹⁰ sputtering,¹¹ or pulsed laser deposition (PLD),¹² among the most widely used. While nonvacuum techniques include solution processing via spin-coating¹³/dip-coating¹⁴/doctor-blade-coating¹⁵/spray^{16,17}/ink-jet printing of the precursor,¹⁸ or electrochemical deposition.¹⁹

Currently, the certified highest efficiency (12.6%) has been achieved using hydrazine-based solution approach,²⁰ although the wide variety of deposition techniques, like coevaporation,^{8,21} sputtering,^{11,22–25} spray,²⁶ spin-coating,^{27,28} or doctor-blade coating,²⁹ have also given efficiencies above 10%.

Historically, solar cells prepared by chemical-based routes have demonstrated better performances than the obtained by physical-based ones. Nevertheless, in the last few years, as illustrated in Figure 1, there has been a remarkable improvement of devices

fabricated through PVD-based approaches like sputtering and coevaporation, which is of great importance from the industrial point of view. In terms of scalability, in general, these vacuum-based processes are very interesting because they can be easily scaled-up with high reproducibility as it has been demonstrated by CIGSe. Regarding coevaporation-based kesterite absorbers, Lee et al.²¹ from IBM reported an 11.6% efficiency device in 2015, and also researchers from the AIST have demonstrated efficiencies as high as 12.3% by using this deposition technique, although with a Ge-incorporated $\text{Cu}_2\text{Zn}(\text{Sn}_{1-x}\text{Ge}_x)\text{Se}_4$ (CZTGSe) kesterite absorber ($\text{Ge}/\text{Ge} + \text{Sn} = 0.22$).⁸ Nevertheless, the available literature on kesterites show that the sputtering is the most widely used PVD-based technique. In this field, IMEC and Nankai University both have reported 10.4% efficiencies for pure selenium CZTSe devices,^{30,31} while IREC and Solar Frontier both have achieved 11.8% efficiency for CZTSe²⁴ and CZTSSe³² respectively, DGIST has reported a 12.3% efficiency CZTSSe device,³³ and the UNSW has reported a certified 11.0% efficiency cell for pure sulfur CZTS.³⁴

In this work, we study the use of advanced MBE (molecular beam epitaxy) systems to grow metallic precursors stacks, alternatively to the sputtering or the conventional thermal evaporation techniques, in combination with the commonly used conventional tubular furnace selenization in order to obtain high quality CZTSe absorbers. In particular, the sputtering and the MBE deposition techniques will be exhaustively studied and compared for the fabrication of high efficiency kesterite solar cell devices. The sputtering deposition is a widely known technique for the easy growth of metallic layers, although the deposition rates, the growth morphology and nucleation, or the roughness, in some cases, can be an issue in the following steps, leading to inhomogeneities in the final layers after the thermal annealing. Nevertheless, the MBE technique can have some advantages to obtain very high quality metallic layers, with an accurate control of the growth due to the ultra-high vacuum conditions ($p < 10^{-8}$ Torr) as well as very high purity.

2 | EXPERIMENTAL

The CZTSe absorbers were synthesized by employing a two-stage sequential process consisting in the deposition of metallic stacks, either by DC-magnetron sputtering (Alliance AC450) or by MBE, followed by a reactive annealing under Se + Sn atmosphere. The structure of the deposited stacks is the following: SLG/Mo/Cu(5 nm)/Sn/Cu/Zn, always in Cu-poor and Zn-rich conditions, as has been recurrently proven to be the optimum to obtain high performance kesterite devices.^{35,36} A calibrated X-ray fluorescence equipment (Fischerscope XVD) was used to control and adjust the goal compositions and thicknesses. All the precursors were doped with a 10-nm-thick layer of Ge, deposited by thermal evaporation technique (Oerlikon Univex 250), based on the good results obtained previously with this approach.²²

Different reactive annealing conditions were performed in order to assess the effect on each type of precursor. These thermal annealings were performed using semi-closed graphite boxes (69 cm^3 in volume) with varying Se quantities from 20 to 100 mg of Se powder and 5 mg of Sn powder, in a conventional three-zone tubular furnace. The

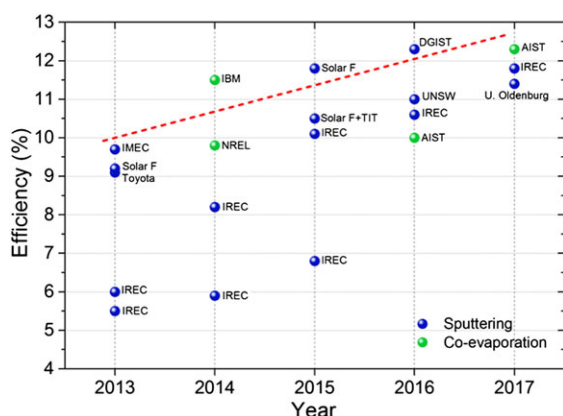


FIGURE 1 Evolution of the efficiency for selected kesterite solar cells fabricated by PVD-based processes (sputtering or coevaporation techniques) in different institutions [Colour figure can be viewed at wileyonlinelibrary.com]

annealing profile consisted in a two-step process; first, 30 minutes at 400°C and 1 mbar (with Ar flux), and second, 15 minutes at different temperatures from 500°C to 575°C and 1000 mbar total Ar pressure. After that, the samples were naturally cooled down until room temperature. Further details can be found elsewhere.^{24,37}

In order to complete the solar cells, a chemical etching with $(\text{NH}_4)_2\text{S}$ was performed to prepare the absorber surface before the growth of the CdS buffer layer (50 nm) by chemical bath deposition (CBD). Immediately after the CdS deposition, the devices were completed with i-ZnO (50 nm) and $\text{In}_2\text{O}_3\text{-SnO}_2$ (ITO, 200 nm) by DC-pulsed sputtering (Alliance CT100). Finally, $3 \times 3 \text{ mm}^2$ solar cells were mechanically scribed using a manual microdiamond scribe (MR200 OEG Optical Metrology). In the case of champion cells, the scribing was made to obtain a total cell area of 0.522 cm^2 , including the deposition of MgF_2 anti-reflective coating and Ag metallic grid.

As-grown CZTSe:Ge absorber layers were characterized using calibrated XRF to determine the composition after the different annealing treatments. In order to assess the impact of the different annealing conditions on the layers morphology, cross-sectional scanning electron microscopy (SEM) (ZEISS Series Auriga) was performed using 5 kV accelerating voltage. Raman scattering measurements were obtained using a homemade Raman system coupled with an iHR320 Horiba Jobin Yvon spectrometer and a solid-state laser with 532 nm excitation wavelength. X-ray diffraction (XRD) was carried out using a PANalytical X'Pert PRO MPD Alpha1 powder diffractometer in Bragg-Brentano $\theta/2\theta$ reflection geometry, from 4 to 145° with step size of 0.017° and integration time of 200 seconds per step, using Cu $\text{K}\alpha_1$ radiation ($\lambda = 1.5406 \text{ \AA}$), and work power 45 kV-40 mA.

Finally, J-V characteristics of the finished solar cell devices were analyzed under simulated AM1.5 illumination (1000 W/m^2 intensity at room temperature) using a calibrated Sun 3000 Class AAA solar simulator (Abet Technologies), as well as the external quantum efficiency (EQE) of the best devices (Bentham PVE300). Additional depth

profiling analysis was performed by GDOES measurements using a Horiba Jobin Yvon GD Profiler 2 spectrometer, equipped with an anode diameter of 4 mm and 19 element channels.

3 | RESULTS AND DISCUSSION

To compare the metallic precursors, Cu/Sn/Cu/Zn stacks were deposited either by sputtering or MBE system. Figure 2 shows the cross-sectional SEM micrographs of both types of precursors, where the MBE-deposited ones are significantly rougher when compared with the sputtered ones. Analyzing in more detail these films, two layers can be clearly distinguished from their morphology, which correspond to Cu-Sn metallic phases or bronzes (in red), and Cu-Zn metallic phases or brasses (in blue). Additional XRD characterization was performed on these layers (see Supporting Information, Figure S2), confirming the presence of the same metallic phases and practically the same relative amounts, mainly Cu_6Sn_5 , Cu_5Zn_8 , and metallic Sn phases. Since the temperatures applied during the precursor deposition are kept below 100°C , the stack structure is what determines the position of the formed alloys, keeping the bronzes at the bottom and the brasses on top. In fact, this strategic stack configuration allows minimizing to some extent the free Sn metallic phases that normally lead to the well-known Sn loss during the reactive annealing treatments.^{36,38} Besides, the precursor morphology is something to pay special attention on, since it could impact to some extent on the final film roughness and morphology but also can affect the composition homogeneity. Actually, recent studies have shown high efficiencies in kesterite devices with relatively simple processing steps through the selenization of very flat and smooth precursors,²⁵ as well as the hydrazine-based approaches that can synthesize very homogeneous layers, which have achieved the highest efficiencies reported for CZTSSe solar cells.²⁰

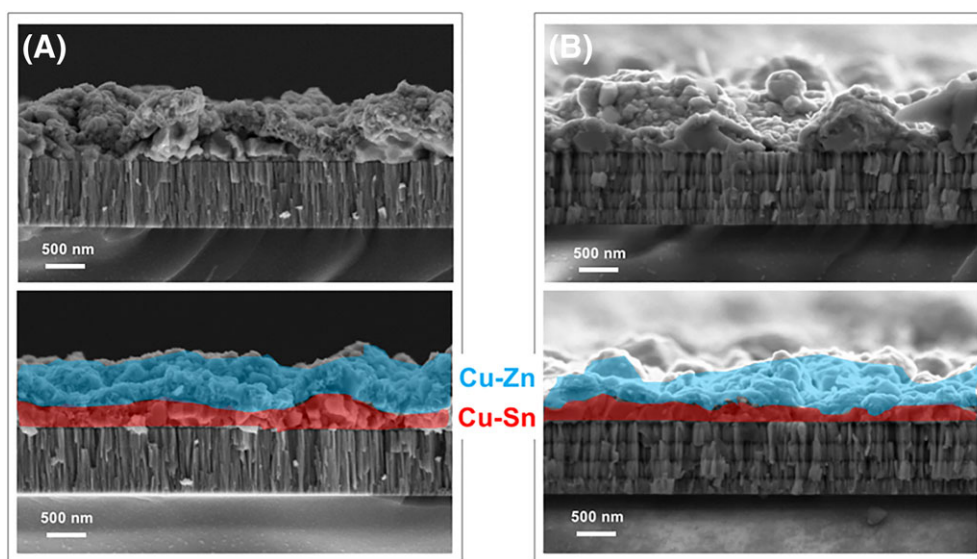


FIGURE 2 Cross-sectional SEM micrographs of metallic stack precursors deposited by A, DC-magnetron sputtering and B, MBE system [Colour figure can be viewed at wileyonlinelibrary.com]

The optimization of the thermal annealing processes is a key factor when the properties of the precursors are modified due to different deposition systems. The porosity, the compactness or the roughness are some of the characteristics that can be affected by the deposition technique, and these have to be considered to adjust the reactive annealing processes, since it can affect the final layer morphology, the degree of molybdenum selenization, the presence of undesired secondary phases, etc.

Therefore, different annealing conditions were tested for both types of metallic precursors, by modifying two of the most relevant selenization parameters: (a) the second step annealing temperature (ie, crystallization temperature) and (b) the selenium quantity, which will impact on the selenium partial pressure during the process. Figure 3 shows the SEM analysis of the samples fabricated using different annealing conditions. Here, the effect of the annealing temperature is assessed (from 500°C to 575°C) for each type of precursor, keeping the Se amount constant (100 mg). As one could expect, the increasing crystallization temperature leads to a gradual increase of the grain size for both types of precursors. Nevertheless, larger grains are systematically obtained for the sputtered precursors (see Figure 3 A), and additionally the degree of selenization of the molybdenum back contact is much lower in this case. This likely indicates a higher porosity of the MBE-deposited precursors, allowing a fast diffusion of the Se vapors towards the back contact, which could be controlled

to some extent by the Se vapor pressure as will be shown below. A reasonable explanation for the different grain growth could be the different nature of the MBE and sputtered precursors; indeed, compared to the former, sputtered films are typically more compact with reasonably higher compressive stress, which is known to act as a driven force for the grain growth during the annealing treatment.^{39,40}

As previously commented, the Se amount introduced during the selenization can be directly related to the Se partial pressure during the process. In Figure 4, a better crystallization with bigger grains is corroborated for the sputtered precursors, while the MBE-deposited ones show a clear overselenization of the back contact with the increasing Se quantity up to 100 mg. This confirms a similar behavior as with the variation of the annealing temperature, although the Se quantity has a greater impact on the molybdenum selenide thickness for the MBE-deposited samples. This consistently observed higher degree of selenization likely reflects a higher reactivity of the MBE-evaporated precursors or porosity.

Further compositional analysis corroborates some of the previous observations. As can be seen in Figure 5, the Se content in the absorbers from sputtered precursors remains practically constant, regardless of the temperature increase or the Se quantity used in the reactive annealing, while it gradually increases for the MBE-deposited samples as both temperature and Se quantity are increased. Thus, this confirms the overselenization previously shown by SEM

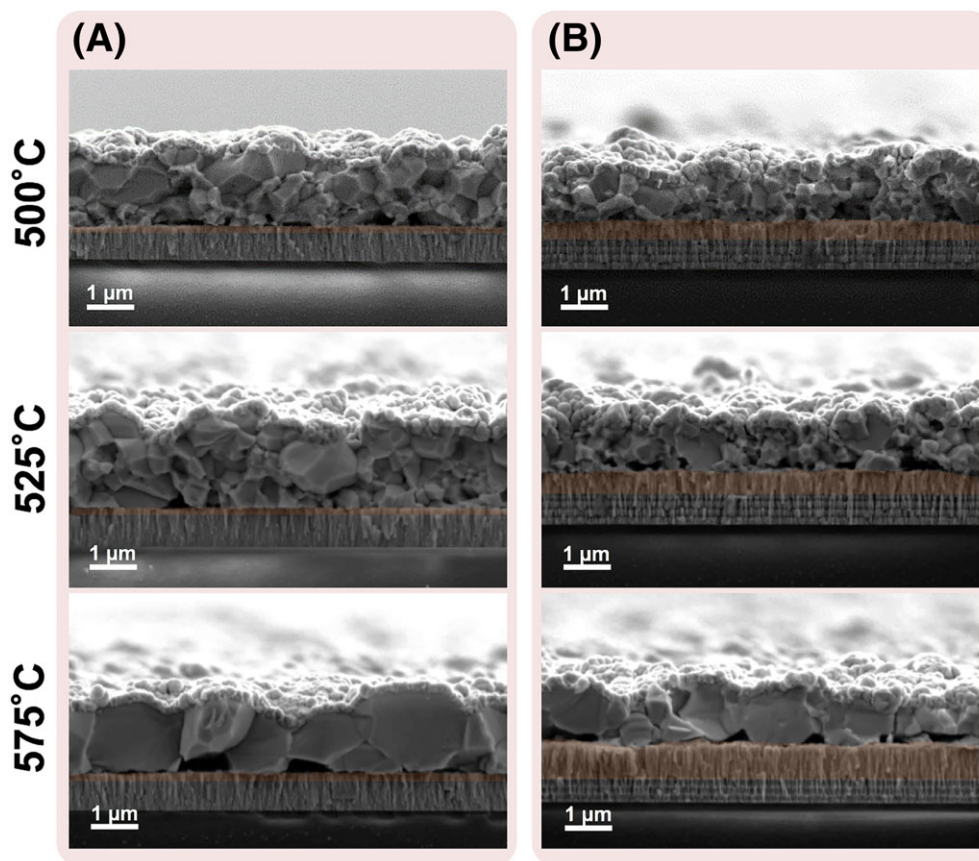


FIGURE 3 SEM analysis showing the effect of the reactive annealing temperature on the layers morphology, from A, sputtered metallic precursors and from B, MBE-deposited metallic precursors. MoSe₂ layer is colored in orange [Colour figure can be viewed at wileyonlinelibrary.com]

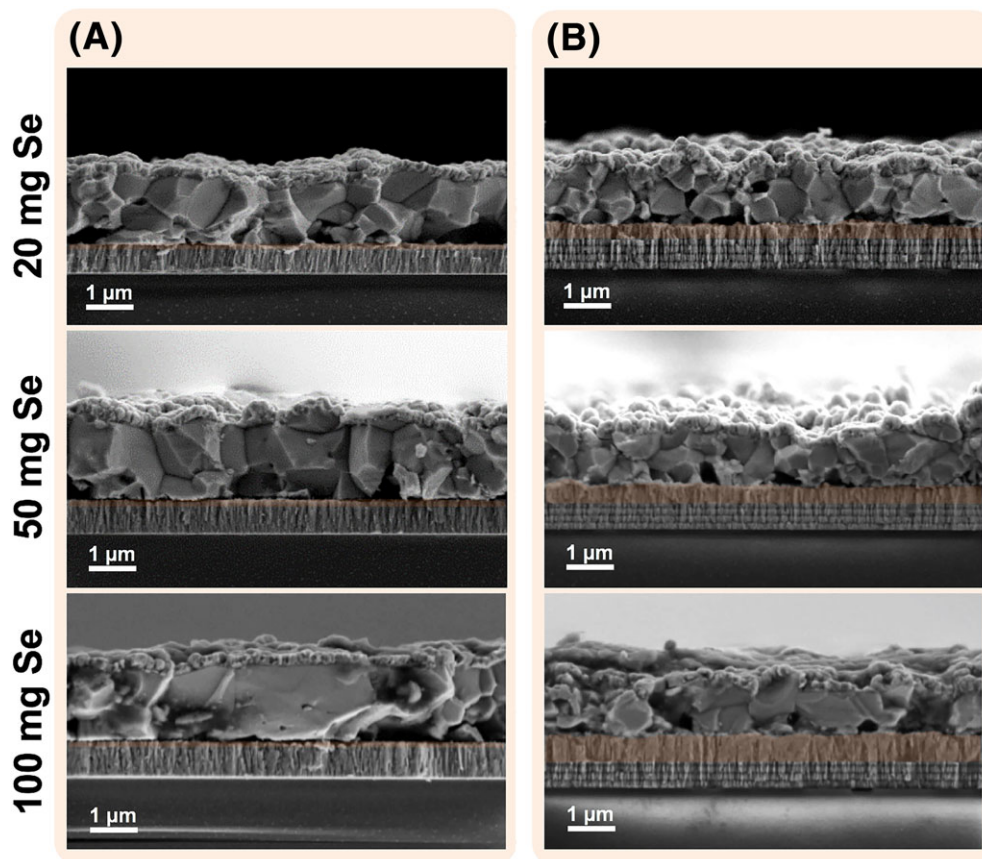


FIGURE 4 SEM analysis showing the impact of the Se quantity used for the reactive annealing process on the layers morphology, from A, sputtered metallic precursors and from B, MBE-deposited metallic precursors. MoSe₂ layer is colored in orange [Colour figure can be viewed at wileyonlinelibrary.com]

analysis, being this type of precursors more susceptible to selenization. Nevertheless, the composition in the case of the sputtered precursors seems not to depend on the variation of the two studied parameters (T and Se quantity).

On the other hand, looking at some characteristic compositional ratios (see Figure 5), intriguingly they show that Sn becomes additionally incorporated with the increasing annealing temperature and Se amount, in particular for the MBE-deposited samples. Cu/Sn and Zn/Sn ratios are significantly reduced as both parameters are increased. As it widely known, Sn tends to be adjusted by means of SnSe₂ presence during the reactive annealing, and probably due to the higher reactivity of the MBE-evaporated precursors, the control of this element becomes even more critical than for the sputtering.

To further investigate the effect of this compositional variations on the structural properties, the crystalline quality or the presence of undesired secondary phases, Raman spectroscopy analysis were performed on the different samples (see Figure S1 in the Supporting Information). Interestingly, rather small differences were observed in terms of crystalline quality, defects, or secondary phases (those detectable with green excitation wavelength, 532 nm). Thus, suggesting a very similar material, structurally speaking.

To eventually see the impact on the device performance, all these layers were made into solar cells and measured under a solar simulator. Figure 6 compares the photovoltaic parameters extracted from

the measured illuminated J-V curves for the two types of samples as the annealing temperature is changed. A similar trend can be observed for the efficiencies and FF of sputtered and MBE-evaporated samples, although the sputtered ones start to deteriorate for the highest temperature (575°C). Looking at the other parameters, in general, we observe quite similar values and trend for the current density (J_{SC}). However, the open-circuit voltage (V_{OC}) remains notably lower for the MBE-deposited precursors.

Additionally, Figure 7 shows how the Se amount during the reactive annealing affects the photovoltaic parameters of the different devices. Clearly, the MBE-evaporated precursors are some more dependent on the Se quantity, showing a slight improvement of the V_{OC} and FF values with the increasing Se, while for the sputtered precursors it has an almost negligible effect.

Intriguingly, the voltage values for all the MBE-deposited samples are remarkably lower when compared with the sputtered ones, regardless of the selenization parameter that has been modified. Due to different system technical requirements for the sputtered and the MBE-deposited precursors, two different soda-lime glass thicknesses were used as well as different Mo depositions for each kind of precursor (the Mo back contact was previously optimized for each type of process, ie, sputtering and MBE, at IREC and AIST, respectively) although they were deposited to obtain the same thicknesses and electrical properties and were both stored in equal conditions.

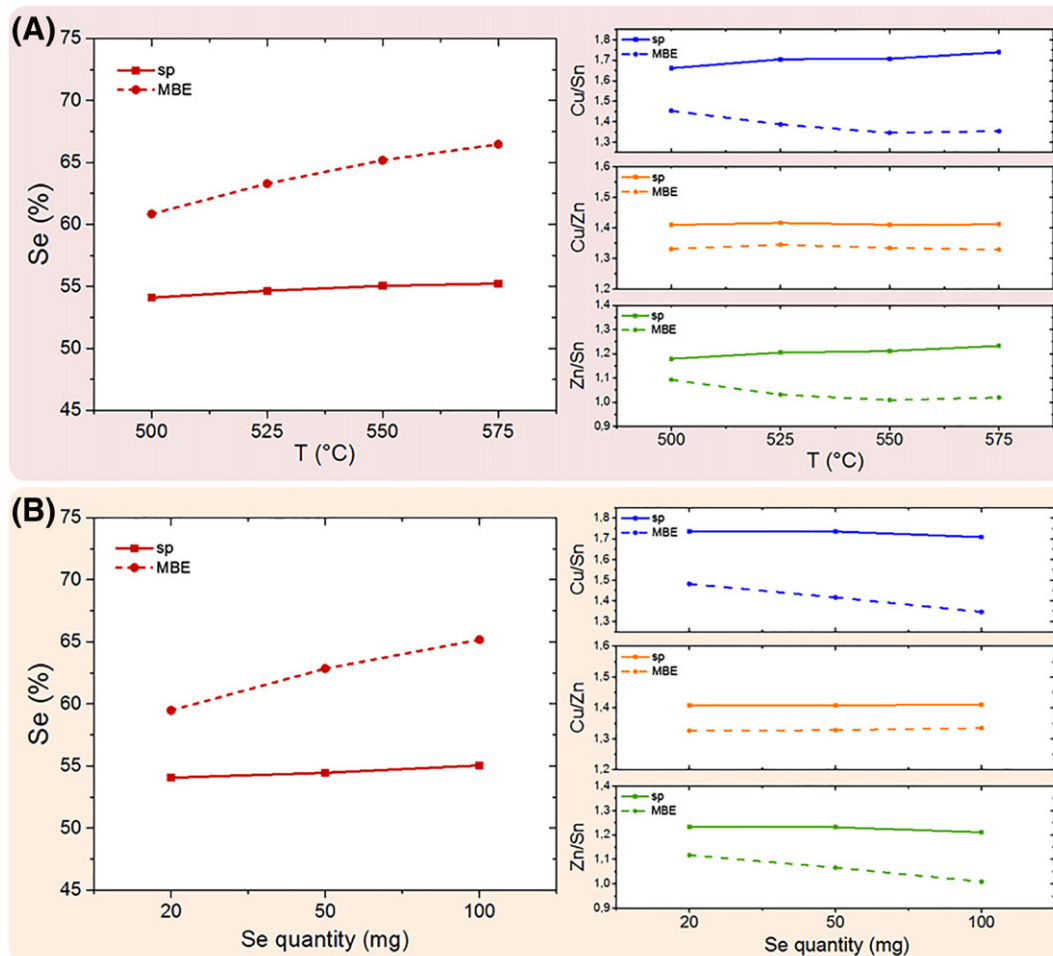


FIGURE 5 XRF compositional analysis (Se % content and relevant compositional ratios) of kesterite absorbers synthesized from sputtered (lines) and MBE-deposited precursors (dashed lines) as function of A, the annealing temperature and B, the Se quantity [Colour figure can be viewed at wileyonlinelibrary.com]

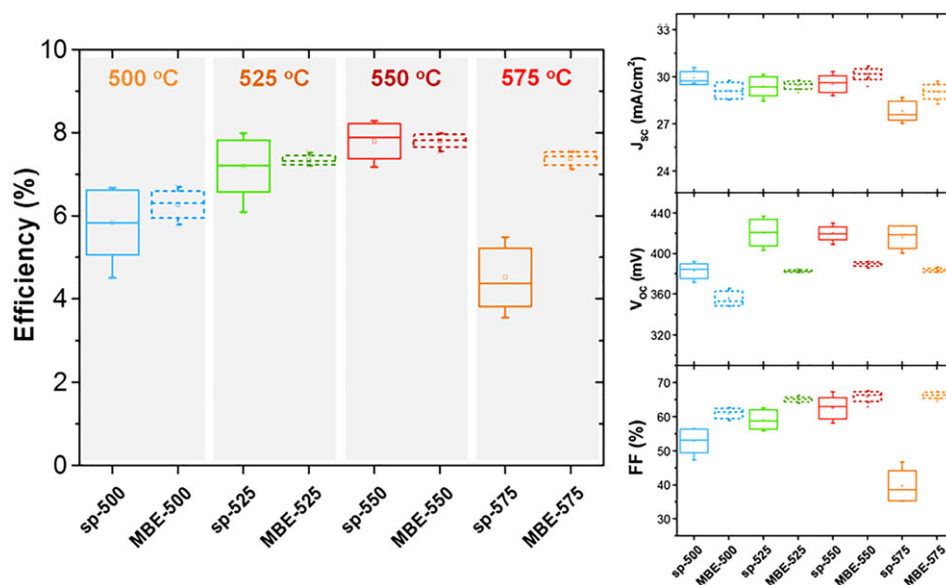


FIGURE 6 Photovoltaic parameters of solar cell devices fabricated from sputtered and MBE-evaporated precursors as function of the reactive annealing temperature. For comparison, the Se quantity remained constant at 100 mg in all these cases [Colour figure can be viewed at wileyonlinelibrary.com]

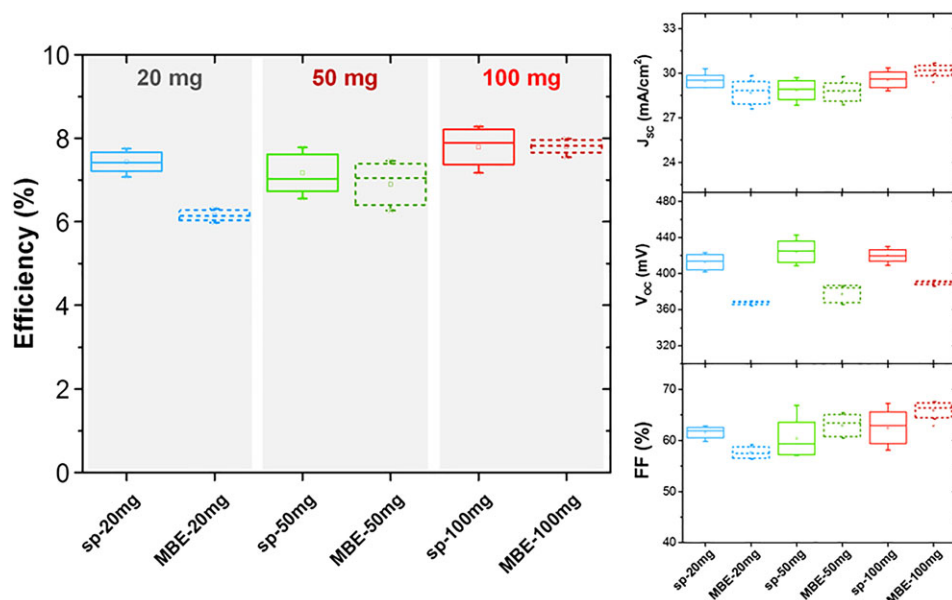


FIGURE 7 Photovoltaic parameters of solar cell devices fabricated from sputtered and MBE-evaporated precursors as function of the Se quantity used for the selenization process. For comparison, the annealing temperature remained constant at 550°C in all these cases [Colour figure can be viewed at wileyonlinelibrary.com]

Specifically, 3-mm glass substrates were used for the sputtering, and 1-mm glass substrates were used for the MBE system. Therefore, the alkali diffusion, especially sodium, is a factor that must be considered. It is well known that sodium plays an important role in controlling the electrical properties, mainly modifying the doping concentration. In particular, sodium increases hole density and leads to higher built-in voltage, thus obtaining higher V_{OC} . Moreover, it can reduce the concentration of certain deep recombination centers, further improving the V_{OC} , and also importantly, it can enhance the FF due to the increased CZTSe conductivity by the higher hole density and mobility.⁴¹ The fact of using a thinner glass substrate together with the use of slightly different Mo layers could probably lead to different sodium dynamics; thus, a nonoptimal sodium diffusion into the CZTSe absorber layer during the synthesis and also considering that all the conditions and parameters of the different fabrication processes are optimized for the thicker substrates. This could reasonably explain the lower voltages systematically obtained for the MBE-evaporated

precursors and also the different evolution of the FF values in both types of samples with the increasing temperature. While the MBE-deposited samples show a gradual improvement of the FF, the sputtered precursors show a sharp drop of this parameter for the highest temperature. Since the temperature is closely related to sodium diffusion, this could be related to an excess of sodium in the second case and still a lack of sodium in the first one. Besides, it is well known that the presence of Na during the reactive annealing strongly influences the grain growth and crystallinity, leading to larger grain sizes and better morphologies.^{42,43} Therefore, this also correlates well with the previous absorbers' SEM characterization showing bigger grains for the sputtered samples, since they are deposited onto thicker glass substrates. In particular, sputtering-based layers show slightly Zn-rich compositions, which have been shown to be optimal to enhance the conversion efficiency⁴⁴; therefore, further studies are needed in order to analyze the impact of the composition in MBE-grown layers.

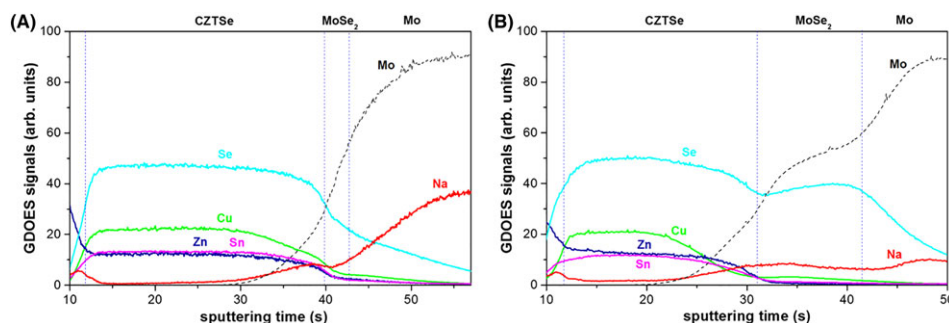


FIGURE 8 GDOES depth profiles of two comparable CZTSe devices fabricated from A, sputtered and B, MBE-deposited precursors. The increase of the Zn signal in the 10 to 12 sputtering seconds at the beginning corresponds to the i-ZnO of the window layer [Colour figure can be viewed at wileyonlinelibrary.com]

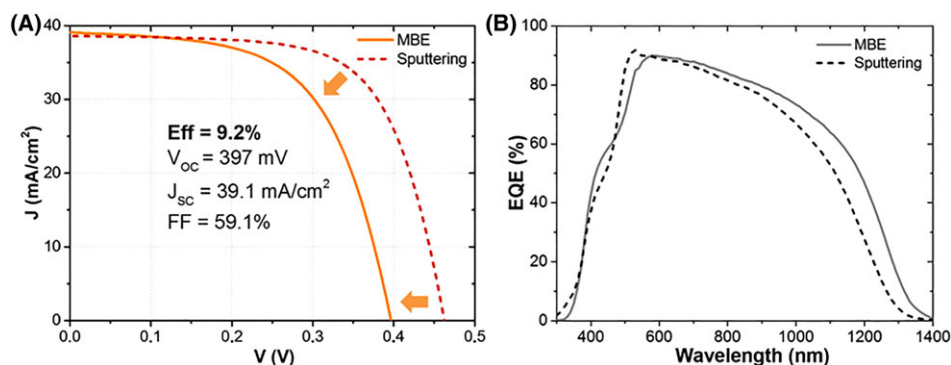


FIGURE 9 Illuminated J-V curve of the champion solar cell from MBE-deposited precursors compared with the sputtered one (A) and EQE (B) [Colour figure can be viewed at wileyonlinelibrary.com]

In order to assess the Na supply from the different substrates, Figure 8 shows the GDOES depth profiles of two complete devices, from a sputtered and from an MBE-deposited precursor, both synthesized using the same annealing conditions (550°C and 100 mg Se). Na amount and distribution in the CZTSe are similar in both devices: Very low amount is detected inside the absorber layers whereas similar Na segregations are observed at the front (CdS/CZTSe) and at the back (CZTSe/MoSe₂) interfaces. However, the quantity of Na detected in the Mo layer is notably higher for the 3-mm glass substrate sample, ie, the sputtering-based one. Therefore, the Na supply and availability during the reactive annealing in this kind of samples could be expected to be higher, which would support our previously stated hypothesis. Additionally, the GDOES profiles show a thicker MoSe₂ interface layer in the MBE sample compared with the sputtered one, in accordance with the SEM cross-sections in Figures 3 and 4.

Further optimizations of the precursor composition, finally led to a conversion efficiency of 9.2% (total area, 0.522 cm²) with MgF₂ anti-reflective coating for MBE-deposited precursors. Figure 9 shows the champion J-V curve and EQE for samples from MBE-evaporated layers, compared with the best sputtering-based cell. This champion sputtering-based solar cell was fabricated in a different batch, using the optimized baseline process, achieving an efficiency greater than 11%, and is shown for comparison. As can be seen, relatively high current densities are achieved, exceeding 39 mA/cm², which are at the same level of the best cells reported so far for the pure selenide CZTSe compound.^{21,25} Nonetheless, V_{OC} and especially FF values remain still lower compared with these record devices. As discussed earlier, this might be explained by a less controlled selenization and a nonoptimal alkali content, which can have a great impact on these solar cell parameters.

In the same vein, Figure 9A shows the clear difference between the two champion solar cells, the one synthesized from MBE-evaporated precursors and the one from sputtered precursors, and the V_{OC} is the main responsible, leading to slightly higher voltage deficits for the MBE system (about 340 mV vs 325 mV as determined by using the Shockley-Queisser limit). Additionally, Figure 9B shows the EQE of these two devices, where a slight difference in the band gap can be seen (1.0 eV for the MBE and 1.04 eV for the sputtering,

estimated from the EQE using the derivative method), although it does not seem of great relevance; this small variation would not totally explain the difference in V_{OC} as well as it could be due to slight compositional differences.

4 | CONCLUSIONS

In this work, the use of MBE-deposited metallic stack precursors has been studied as an alternative for the commonly used sputtered or thermally evaporated precursors to synthesize CZTSe photovoltaic absorbers. Apparently, MBE-deposited precursors exhibit similar properties and the presence of the same metallic phases compared to the sputtered ones. Nevertheless, the first ones show a different behavior during the reactive annealing, incorporating higher Se quantities with the concomitant thicker MoSe₂ layer at the Mo/CZTSe interface, and exchanging relevant amounts of Sn with the annealing atmosphere, probably due to a higher reactivity of these type of precursors. Regarding solar cell devices, the main efficiency limitations come from the V_{OC} and FF, most likely due to a nonoptimal alkali supply and/or composition, and a less controlled selenization. Finally, in the first optimization, a 9.2% efficiency cell (9.8% efficiency, active area) is achieved, demonstrating that MBE systems are a suitable technique to fabricate metallic stack precursors and obtain high performance solar cell devices, at the level of widely used techniques like sputtering or thermal evaporation. The work presented here opens promising perspectives for the future development of kesterites, giving alternative approaches to fabricate high efficiency kesterite solar cells.

ACKNOWLEDGEMENTS

This research was supported by the H2020 Programme and H2020 Societal Challenges under the STARCELL Project (H2020-NMBP-03-2016-720907), by Secretaría de Estado de Investigación, Desarrollo e Innovación, MINECO (Ministerio de Economía y Competitividad de España) under the WINCOST Project (ENE2016-80788-C5-1-R) and IGNITE Project (ENE2017-87671-C3-1-R), by the European Regional Development Funds (ERDF, FEDER Programa Competitivitat de Catalunya 2007–2013). Authors from IREC and the University of Barcelona belong to the SEMS (Solar Energy Materials and Systems)

Consolidated Research Group of the "Generalitat de Catalunya" (Agència de Gestió d'Ajuts Universitaris i de Recerca, Ref. 2017 SGR 862). S.G. thanks the Ministerio de Economía y Competitividad (MINECO) for the FPI fellowship (BES-2014-068533).

ORCID

Sergio Giraldo  <https://orcid.org/0000-0003-4881-5041>

REFERENCES

- Kaur K, Kumar N, Kumar M. Strategic review of interface carrier recombination in earth abundant Cu–Zn–Sn–S–Se solar cells: current challenges and future prospects. *J Mater Chem A*. 2017;5(7):3069–3090. <https://doi.org/10.1039/C6TA10543B>
- Polizzotti A, Repins IL, Noufi R, Wei S-H, Mitzi DB. The state and future prospects of kesterite photovoltaics. *Energ Environ Sci*. 2013;6(11):3171. <https://doi.org/10.1039/c3ee41781f>
- Huang TJ, Yin X, Qi G, Gong H. CZTS-based materials and interfaces and their effects on the performance of thin film solar cells. *Phys Status Solidi Rapid Res Lett*. 2014;8(09):735–762. <https://doi.org/10.1002/pssr.201409219>
- Wadia C, Alivisatos AP, Kammen DM. Materials availability expands the opportunity for large-scale photovoltaics deployment. *Environ Sci Technol*. 2009;43(6):2072–2077. <https://doi.org/10.1021/es8019534>
- Seol J, Lee S, Lee J, Nam H, Kim K. Electrical and optical properties of Cu₂ZnSnS thin films prepared by rf magnetron sputtering process. *Sol Energy Mater Sol Cells*. 2003;75(1–2):155–162. [https://doi.org/10.1016/S0927-0248\(02\)00127-7](https://doi.org/10.1016/S0927-0248(02)00127-7)
- He J, Sun L, Chen S, Chen Y, Yang P, Chu J. Composition dependence of structure and optical properties of Cu₂ZnSn(S,Se)₄ solid solutions: an experimental study. *J Alloys Compd*. 2012;511(1):129–132. <https://doi.org/10.1016/j.jallcom.2011.08.099>
- Ahn S, Jung S, Gwak J, et al. Determination of band gap energy (E_g) of Cu₂ZnSnSe₄ thin films: on the discrepancies of reported band gap values. *Appl Phys Lett*. 2010;97(2):021905. <https://doi.org/10.1063/1.3457172>
- Kim S, Kim KM, Tampo H, Shibata H, Niki S. Improvement of voltage deficit of Ge-incorporated kesterite solar cell with 12.3% conversion efficiency. *Appl Phys Express*. 2016;9(10):1–5. <https://doi.org/10.7567/APEX.9.102301>
- Guc M, Caballero R, Lisunov KG, et al. Disorder and variable-range hopping conductivity in Cu₂ZnSnS₄ thin films prepared by flash evaporation and post-thermal treatment. *J Alloys Compd*. 2014;596:140–144. <https://doi.org/10.1016/J.JALLCOM.2014.01.177>
- Ranjbar S, Brammertz G, Vermang B, et al. Effect of Sn/Zn/Cu precursor stack thickness on two-step processed kesterite solar cells. *Thin Solid Films*. 2017;633:127–130. <https://doi.org/10.1016/J.TSF.2016.09.040>
- Giraldo S, Neuschitzer M, Thersleff T, et al. Large efficiency improvement in Cu₂ZnSnSe₄ solar cells by introducing a superficial Ge nanolayer. *Adv Energy Mater*. 2015;5(21):1501070. <https://doi.org/10.1002/aenm.201501070>
- Cazzaniga A, Crovetto A, Yan C, et al. Ultra-thin Cu₂ZnSnS₄ solar cell by pulsed laser deposition. *Sol Energy Mater Sol Cells*. 2017;166:91–99. <https://doi.org/10.1016/J.SOLMAT.2017.03.002>
- Todorov TK, Reuter KB, Mitzi DB. High-efficiency solar cell with earth-abundant liquid-processed absorber. *Adv Mater*. 2010;22(20):E156–E159. <https://doi.org/10.1002/adma.200904155>
- Sun Y, Zong K, Zheng H, et al. Ethylene glycol-based dip coating route for the synthesis of Cu₂ZnSnS₄ thin film. *Mater Lett*. 2013;92:195–197. <https://doi.org/10.1016/J.MATLET.2012.10.120>
- Dong H, Schnabel T, Ahlswede E, Feldmann C. Polyol-mediated synthesis of Cu₂ZnSn(S,Se)₄ kesterite nanoparticles and their use in thin-film solar cells. *Solid State Sci*. 2014;29:52–57. <https://doi.org/10.1016/J.SOLIDSTATESCIENCES.2014.01.006>
- Espindola-Rodriguez M, Placidi M, Vigil-Galán O, et al. Compositional optimization of photovoltaic grade Cu₂ZnSnS₄ films grown by pneumatic spray pyrolysis. *Thin Solid Films*. 2013;535:67–72. <https://doi.org/10.1016/J.TSF.2012.12.082>
- Carrete A, Shavel A, Fontane X, et al. Antimony-based ligand exchange to promote crystallization in spray-deposited Cu₂ZnSnSe₄ solar cells. *J Am Chem Soc*. 2013;135(43):15982–15985. <https://doi.org/10.1021/ja4068639>
- Colina M, Bailo E, Medina-Rodríguez B, et al. Optimization of ink-jet printed precursors for Cu₂ZnSn(S,Se)₄ solar cells. *J Alloys Compd*. 2018;735:2462–2470. <https://doi.org/10.1016/J.JALLCOM.2017.12.035>
- Vauche L, Risch L, Sánchez Y, et al. 8.2% Pure selenide kesterite thin-film solar cells from large-area electrodeposited precursors. *Prog Photovoltaics Res Appl*. 2016;24(1):38–51. <https://doi.org/10.1002/pip.2643>
- Wang W, Winkler MT, Gunawan O, et al. Device characteristics of CZTSSe thin-film solar cells with 12.6% efficiency. *Adv Energy Mater*. 2014;4(7):1301465. <https://doi.org/10.1002/aenm.201301465>
- Lee YS, Gershon T, Gunawan O, et al. Cu₂ZnSnSe₄ thin-film solar cells by thermal co-evaporation with 11.6% efficiency and improved minority carrier diffusion length. *Adv Energy Mater*. 2015;5(7):1401372. <https://doi.org/10.1002/aenm.201401372>
- Giraldo S, Thersleff T, Larramona G, et al. Cu₂ZnSnSe₄ solar cells with 10.6% efficiency through innovative absorber engineering with Ge superficial nanolayer. *Prog Photovoltaics Res Appl*. 2016;24(10):1359–1367. <https://doi.org/10.1002/pip.2797>
- Giraldo S, Neuschitzer M, Placidi M, Pistor P, Perez-Rodriguez A, Saucedo E. Cu₂ZnSnSe₄-based solar cells with efficiency exceeding 10% by adding a superficial Ge nanolayer: the interaction between Ge and Na. *IEEE J Photovoltaics*. 2016;6(3):754–759. <https://doi.org/10.1109/JPHOTOV.2016.2535236>
- Giraldo S, Saucedo E, Neuschitzer M, et al. How small amounts of Ge modify the formation pathways and crystallization of kesterites. *Energ Environ Sci*. 2018;11(3):582–593. <https://doi.org/10.1039/c7ee02318a>
- Taskesen T, Neerken J, Schoneberg J, et al. Device characteristics of an 11.4% CZTSe solar cell fabricated from sputtered precursors. *Adv Energy Mater*. February 2018;8(16):1703295. <https://doi.org/10.1002/aenm.201703295>
- Larramona G, Levchenko S, Bourdais S, et al. Fine-tuning the Sn content in CZTSSe thin films to achieve 10.8% solar cell efficiency from spray-deposited water-ethanol-based colloidal inks. *Adv Energy Mater*. 2015;5(24):1501404. <https://doi.org/10.1002/aenm.201501404>
- Kim J, Hiroi H, Todorov TK, et al. High efficiency Cu₂ZnSn(S,Se)₄ solar cells by applying a double In₂S₃/CdS emitter. *Adv Mater*. 2014;26(44):7427–7431. <https://doi.org/10.1002/adma.201402373>
- Haass SG, Diethelm M, Werner M, Bissig B, Romanyuk YE, Tiwari AN. 11.2% efficient solution processed kesterite solar cell with a low voltage deficit. *Adv Energy Mater*. 2015;5(18):1500712. <https://doi.org/10.1002/aenm.201500712>
- Schnabel T, Abzieher T, Friedlmeier TM, Ahlswede E. Solution-based preparation of Cu₂ZnSn(S,Se)₄ for solar cells—comparison of SnSe₂

- and elemental Se as chalcogen source. *IEEE J Photovoltaics*. 2015;5(2):670-675. <https://doi.org/10.1109/JPHOTOV.2015.2392935>
30. Oueslati S, Brammertz G, Buffière M, et al. Physical and electrical characterization of high-performance $\text{Cu}_2\text{ZnSnSe}_4$ based thin film solar cells. *Thin Solid Films*. 2015;582:224-228. <https://doi.org/10.1016/j.tsf.2014.10.052>
 31. Li J, Wang H, Wu L, et al. Growth of $\text{Cu}_2\text{ZnSnSe}_4$ film under controllable Se vapor composition and impact of low Cu content on solar cell efficiency. *ACS Appl Mater Interfaces*. 2016;8(16):10283-10292. <https://doi.org/10.1021/acsami.6b00081>
 32. Hiroi H, Sakai N, Iwata Y, Kato T, Sugimoto H. Impact of buffer layer on kesterite solar cells. 2015 IEEE 42nd Photovolt Spec Conf. June 2015: 1-4. DOI:<https://doi.org/10.1109/PVSC.2015.7356415>
 33. Kim J, Kim GY, Son D-H, et al. High photo-conversion efficiency $\text{Cu}_2\text{ZnSn(S,Se)}_4$ thin-film solar cells prepared by compound-precursors and metal-precursors. *Sol Energy Mater sol Cells*. 2018;183:129-136. <https://doi.org/10.1016/J.SOLMAT.2018.03.050>
 34. Green MA, Hishikawa Y, Dunlop ED, Levi DH, Hohl-Ebinger J, Ho-Bailie AWY. Solar cell efficiency tables (version 51). *Prog Photovoltaics Res Appl*. 2018;26(1):3-12. <https://doi.org/10.1002/pip.2978>
 35. Becerril-Romero I, Giraldo S, López-Marino S, et al. Vitreous enamel as sodium source for efficient kesterite solar cells on commercial ceramic tiles. *Sol Energy Mater Sol Cells*. 2016;154:11-17. <https://doi.org/10.1016/j.solmat.2016.04.035>
 36. Fairbrother A, Fontané X, Izquierdo-Roca V, et al. Secondary phase formation in Zn-rich $\text{Cu}_2\text{ZnSnSe}_4$ -based solar cells annealed in low pressure and temperature conditions. *Prog Photovoltaics Res Appl*. 2014;22(4):479-487.
 37. Giraldo S, Ruiz CM, Espíndola-Rodríguez M, et al. Optical and electrical properties of In-doped $\text{Cu}_2\text{ZnSnSe}_4$. *Sol Energy Mater Sol Cells*. 2016;151:44-51. <https://doi.org/10.1016/j.solmat.2016.02.024>
 38. Redinger A, Berg DM, Dale PJ, Siebentritt S. The consequences of kesterite equilibria for efficient solar cells. *J Am Chem Soc*. 2011;133(10):3320-3323. <https://doi.org/10.1021/ja111713g>
 39. Malerba C, Valentini M, Azanza Ricardo CL, et al. Blistering in $\text{Cu}_2\text{ZnSnS}_4$ thin films: correlation with residual stresses. *Mater Des*. 2016;108:725-735. <https://doi.org/10.1016/j.matdes.2016.07.019>
 40. Mainz R, Rodriguez-Alvarez H, Klaus M, et al. Sudden stress relaxation in compound semiconductor thin films triggered by secondary phase segregation. *Phys Rev B - Condens Matter Mater Phys*. 2015;92(15):155310. <https://doi.org/10.1103/PhysRevB.92.155310>
 41. Li JV, Kuciauskas D, Young MR, Repins IL. Effects of sodium incorporation in Co-evaporated $\text{Cu}_2\text{ZnSnSe}_4$ thin-film solar cells. *Appl Phys Lett*. 2013;102(16):163905. <https://doi.org/10.1063/1.4802972>
 42. Sutter-Fella CM, Stükelberger JA, Hagendorfer H, et al. Sodium assisted sintering of chalcogenides and its application to solution processed $\text{Cu}_2\text{ZnSn(S,Se)}_4$ thin film solar cells. *Chem Mater*. 2014;26(3):1420-1425. <https://doi.org/10.1021/cm403504u>
 43. Johnson M, Baryshev SV, Thimsen E, et al. Alkali-metal-enhanced grain growth in $\text{Cu}_2\text{ZnSnS}_4$ thin films. *Energ Environ Sci*. 2014;7(6):1931-1938. <https://doi.org/10.1039/C3EE44130J>
 44. Dimitrievska M, Fairbrother A, Saucedo E, Pérez-Rodríguez A, Izquierdo-Roca V. Secondary phase and Cu substitutional defect dynamics in kesterite solar cells: impact on optoelectronic properties. *Sol Energy Mater Sol Cells*. 2016;149:304-309. <https://doi.org/10.1016/j.solmat.2016.01.029>

SUPPORTING INFORMATION

Additional supporting information may be found online in the Supporting Information section at the end of the article.

How to cite this article: Giraldo S, Kim S, Andrade-Arvizu JA, et al. Study and optimization of alternative MBE-deposited metallic precursors for highly efficient kesterite CZTSe:Ge solar cells. *Prog Photovolt Res Appl*. 2019;27:779-788. <https://doi.org/10.1002/pip.3147>